Supplement of Geosci. Model Dev., 19, 8627–8649, 2026
https://doi.org/10.5194/gmd-19-8627-2026-supplement

Geoscientific
Model Development
Open Access

Supplement of

Multi-season evaluation of temperature and wind in the marine boundary layer along the United States northeast coast in the High-Resolution Rapid Refresh model

Bianca Adler et al.

Correspondence to: Bianca Adler (bianca.adler@colorado.edu)

S1 Specifications of input data for TROPoe and WINDoe retrievals

Table S1 overviews instrument manufacturers and specifications for the remote sensing instruments used as input to TROPoe and WINDoe.

Table S1. Overview of manufacturer, variables of interest and spatial resolution and maximum range of the variables of interest from the remote sensing instruments that are used as input to WINDoe and TROPoe. For the radar wind profilers, specification for high- and low-resolution model are given with the latter in brackets. Horizontal wind components are denoted with u and v, radial velocity along the line of sight with rv, and cloud base height with CBH. Maximum range is the theoretical range that can be achieved based on the settings, the actual range depends on atmospheric conditions and is usually lower.

Site	Instrument	Manufacturer, model	Variable of interest	Spatial resolution (m)	Maximum range (m)
NANT	Radar wind profiler	Built by NOAA Physical Sciences Laboratory, 915 MHz	u, v	58 (97)	121-2,925 (164-6,097)
	Scanning Doppler lidar	Halo Photonics, XR+	rv	30	15-12,000
	Profiling Doppler lidar	Vaisala, WindCube V2.1	u, v	20	47-197
	Infrared Spectrometer	LRTech, ASSIST-II	radiance	N/A	N/A
	Ceilometer	Vaisala, CL51	CBH	5	40-13,000
BLOC	Radar wind profiler	Built by NOAA Physical Sciences Laboratory, 915 MHz	u, v	58 (97)	121-2,925 (164-6,097)
	Scanning Doppler lidar	Halo Photonics, XR	rv	30	15-6,000
	Profiling Doppler lidar	Vaisala, WindCube V1	u, v	20	40-220
	Infrared Spectrometer	LRTech, ASSIST-II	radiance	N/A	N/A
	Ceilometer	Vaisala, CL51	CBH	5	40-13,000
RHOD	Radar wind profiler	Vaisala, LAP-3000 915 MHz	u, v	62 (97)	103-2,788 (195-6,031)
	Scanning Doppler lidar	SgurrEnergy, Galion	rv	30	15-6,000
	Profiling Doppler lidar	ZX Lidars, ZephIR-300	u, v	20	10-280
	Infrared Spectrometer	LRTech, ASSIST-II	radiance	N/A	N/A

S2 Comparison of WINDoe retrievals with individual input data

We use WINDoe to combine wind speed profile information from four different data sets, namely high- and low-resolution radar wind profiler data and scanning and profiling lidar data. Table S2 overviews the data sets used for creating the WINDoe retrievals. Each of these data sets has different specifics in terms of scan volume, vertical range, and temporal resolution. In addition the lidars and radar wind profilers are sensitive to completely different scatterers. It thus cannot be expected that they all provide exactly the same wind speed profiles. We compare the wind speed retrieved with WINDoe with the wind speed data from the individual inputs, which are available on Wind Data Hub.

Table S2. Data sets combined in the WINDoe retrieval. For each site the instrument type, naming convention on the Wind Data Hub and DOI are given. Data sets can be accessed online by using the naming convention as in this example: https://wdh.energy.gov/ds/wfip3/rhod.sonic.z01.c0.

Site	Radar wind profiler	Scanning Doppler lidar	Profiling Doppler lidar	Surface tower
NANT	nant.rwp.z01.c1 10.21947/2569390	nant.lidar.z01.00 10.21947/2228417	nant.lidar.z03.b0 10.21947/2447059	nant.rad.z01.a0 10.21947/2323882
BLOC	bloc.rwp.z01.c1 10.21947/2569230	bloc.lidar.z01.a0 10.21947/2229436	bloc.lidar.z03.c0 10.21947/2229426	bloc.met.z01.c1 10.21947/2569867
RHOD	rhod.rwp.z01.00 10.21947/2229548	rhod.lidar.z01.a0 10.21947/2228755	rhod.lidar.z03.00 10.21947/2228964	rhod.sonic.z01.c0 10.21947/2307824

Figure S1 shows the relationship between the WINDoe wind speed on the y-axis and the wind speed from the individual inputs on the x-axis at all 3 sites in the lowest 1500 m. Data were linearly interpolated on the same height grid with 10 m grid spacing and to the same hourly time stamps. The correlation is very high, with Pearson correlation coefficients regularly exceeding 0.95, and neither the radar wind profiler nor scanning lidar data sets show a systematic bias. Only at the low heights where the profiling lidar provides information, retrieved wind speed are slightly lower (by about -0.2 $\mathrm{m\,s^{-1}}$) than the input data. Mean absolute errors (MAE) are mostly well below $1\ \mathrm{ms^{-1}}$, with the exception of the RHOD where MAE are close to 1 $\mathrm{m\,s^{-1}}$. This means that the differences between the retrieved wind speed and the individual input data is within the uncertainty of the retrieved profiles where the 1-σ uncertainty is between 0.8 and 1.5 $\mathrm{m\,s^{-1}}$ in the lowest 1500 m on the average.

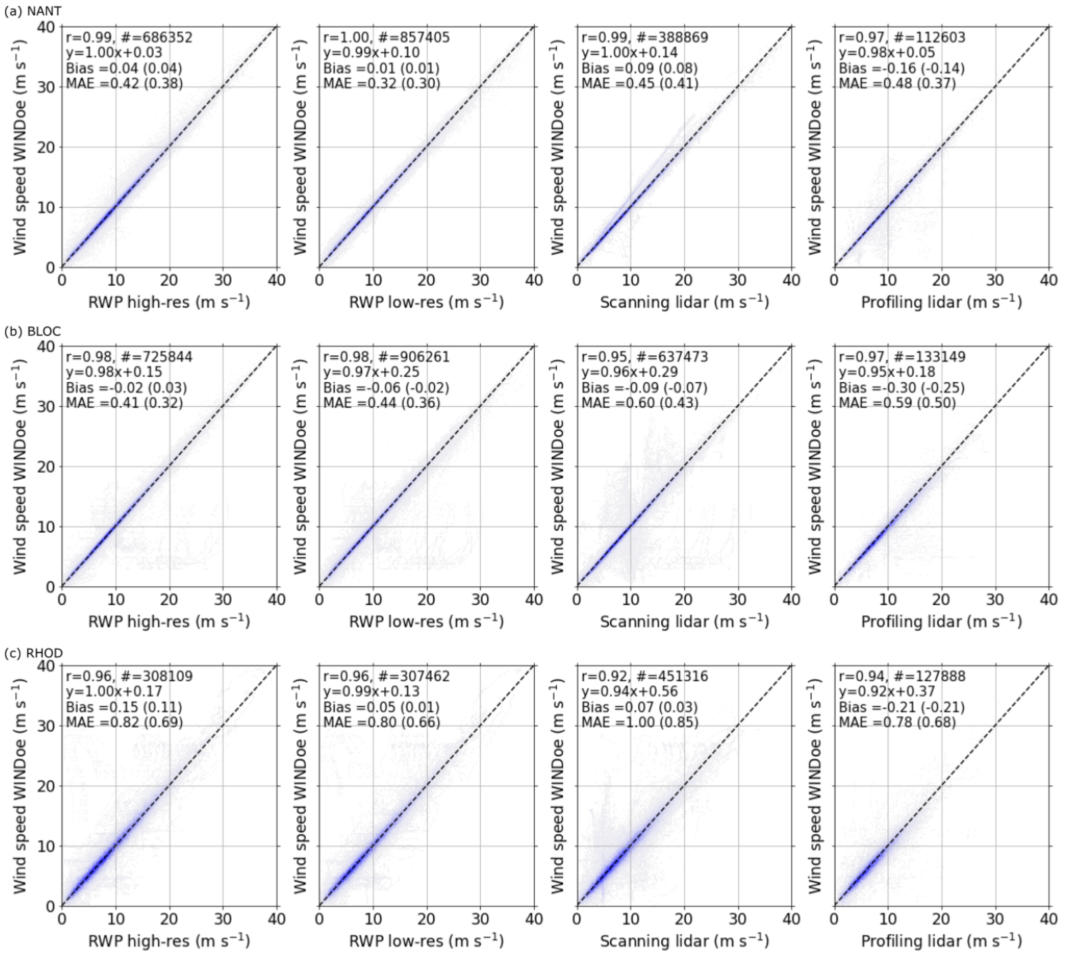

Figure S1. Relationship between wind speed from the WINDoe retrieval and wind speed from the individual input sources which are radar wind profiler high-resolution mode (RWP high-res), radar wind profiler low-resolution model (RWP low-res), scanning lidar, and profiling lidar. Data are interpolated to a 10-m vertical height grid and 60 min temporal resolution. Only data below 1500 m are shown. Values in the upper left corner indicate Pearson correlation coefficient r, number of samples, line of best fit, bias, and mean absolute error MAE. The values in the bracket for bias and MAE are computed for data within the interquartile range.

S3 Comparison of OSTIA SST with in situ buoy measurements

Daily values of OSTIA SST at the grid points closest to the location of two buoys was extracted. Buoyz01 was located in the southern part of the investigation area further offshore and Buoy44085 was located closer to the coast in the northern part of the area. Daily averages of the buoy water temperature measurements were computed and compared against the OSTIA SST (Fig. S2).

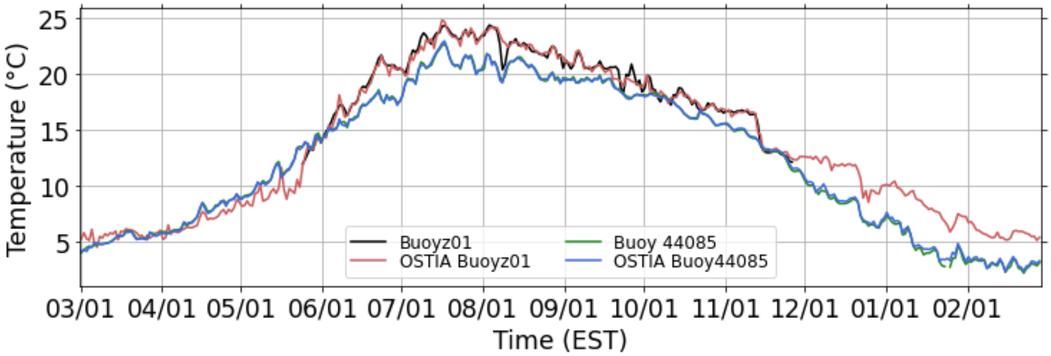

Figure S2. Time series of in situ water temperature measured at buoys and OSTIA sea surface temperature (SST) at grid points closest to the buoy locations during the investigation period. Data from Buoyz01 was only available between the end of May and the end of November 2024.

S4 Composites of wind and temperature profiles at BLOC and RHOD

Monthly composite of the observed and simulated diurnal cycle of wind and temperature at BLOC and RHOD are computed using forecast hour 12 of the HRRR model. In addition, monthly composites of the difference in wind and temperature (model minus observations) are computed.

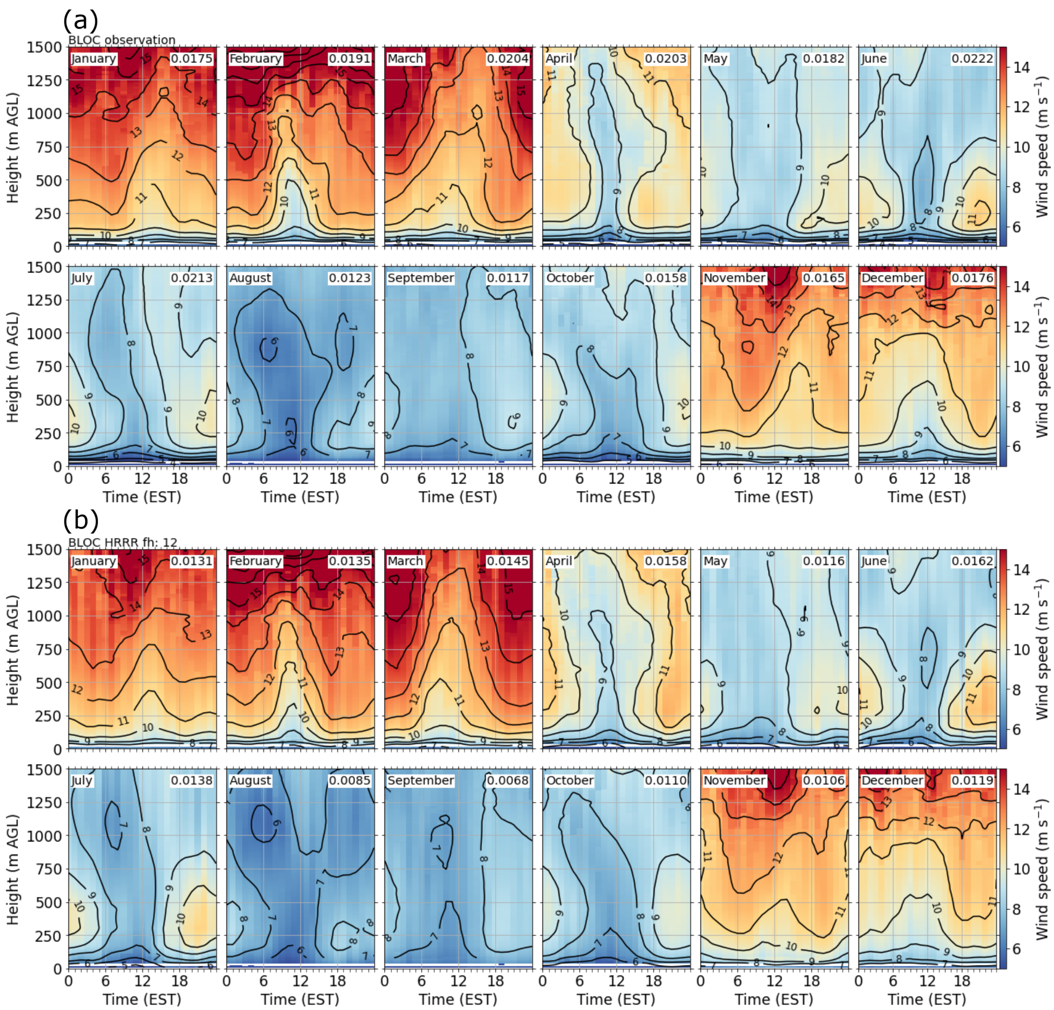

Figure S3. Monthly mean composites of (a) observed and (b) simulated horizontal wind speed (shading and contours) across the full diurnal range at BLOC. In (b), forecast hour 12 of the HRRR model is shown. Only times and heights where both model data and observations were available were used for computing the composites, and availability had to be at least 25 % for a time/height pair to be plotted. The number in the upper right corner of each subplot indicates the monthly mean shear in s^{-1} in the layer 50 to 200 m. Time is given in Eastern Standard Time (EST = UTC - 5 hours).

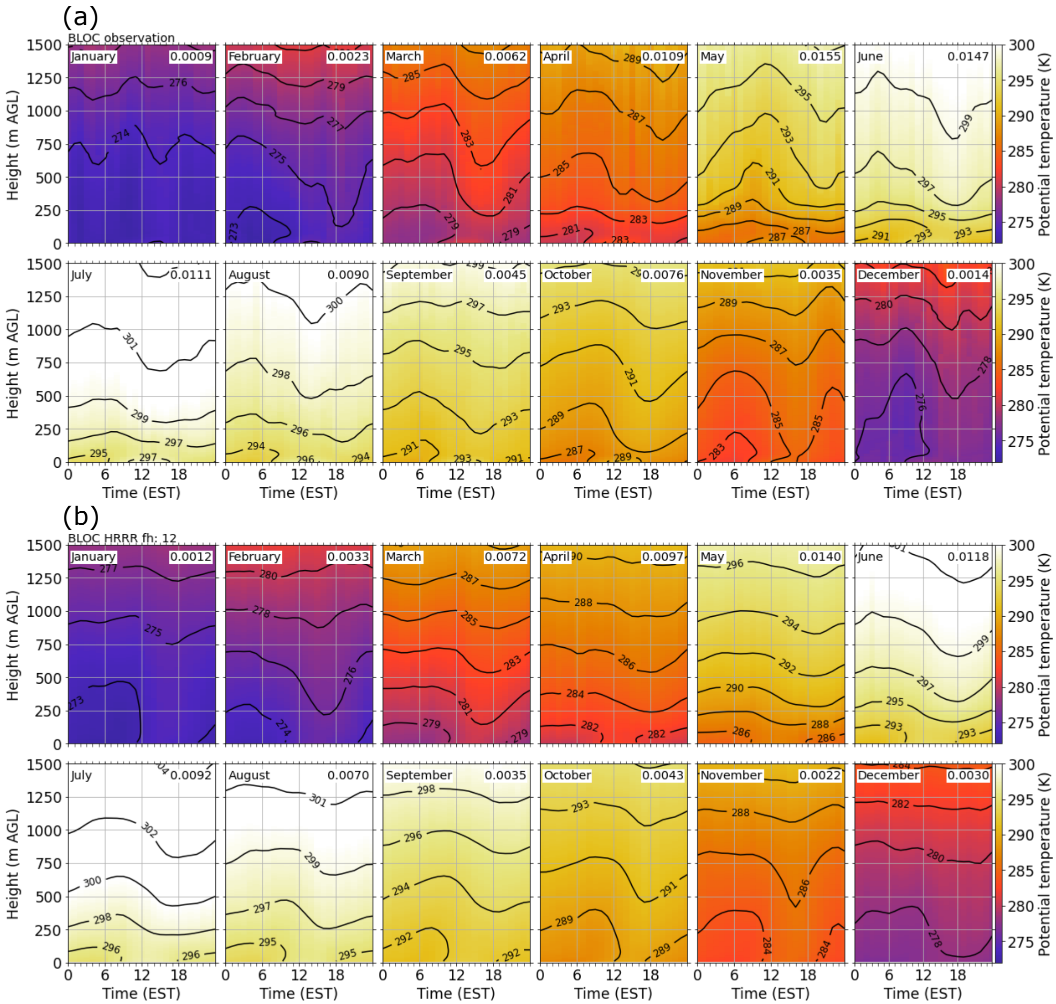

Figure S4. Monthly mean composites of (a) observed and (b) simulated potential temperature (shading and contours) across the full diurnal range at BLOC. In (b), forecast hour 12 of the HRRR model is shown. Only times and heights where both model data and observations were available were used for computing the composites, and availability had to be at least 25 % for a time/height pair to be plotted. The number in the upper right corner of each subplot indicates the monthly mean static stability in K m^{-1} in the layer 50 m to 200 m. Time is given in Eastern Standard Time (EST = UTC - 5 hours).

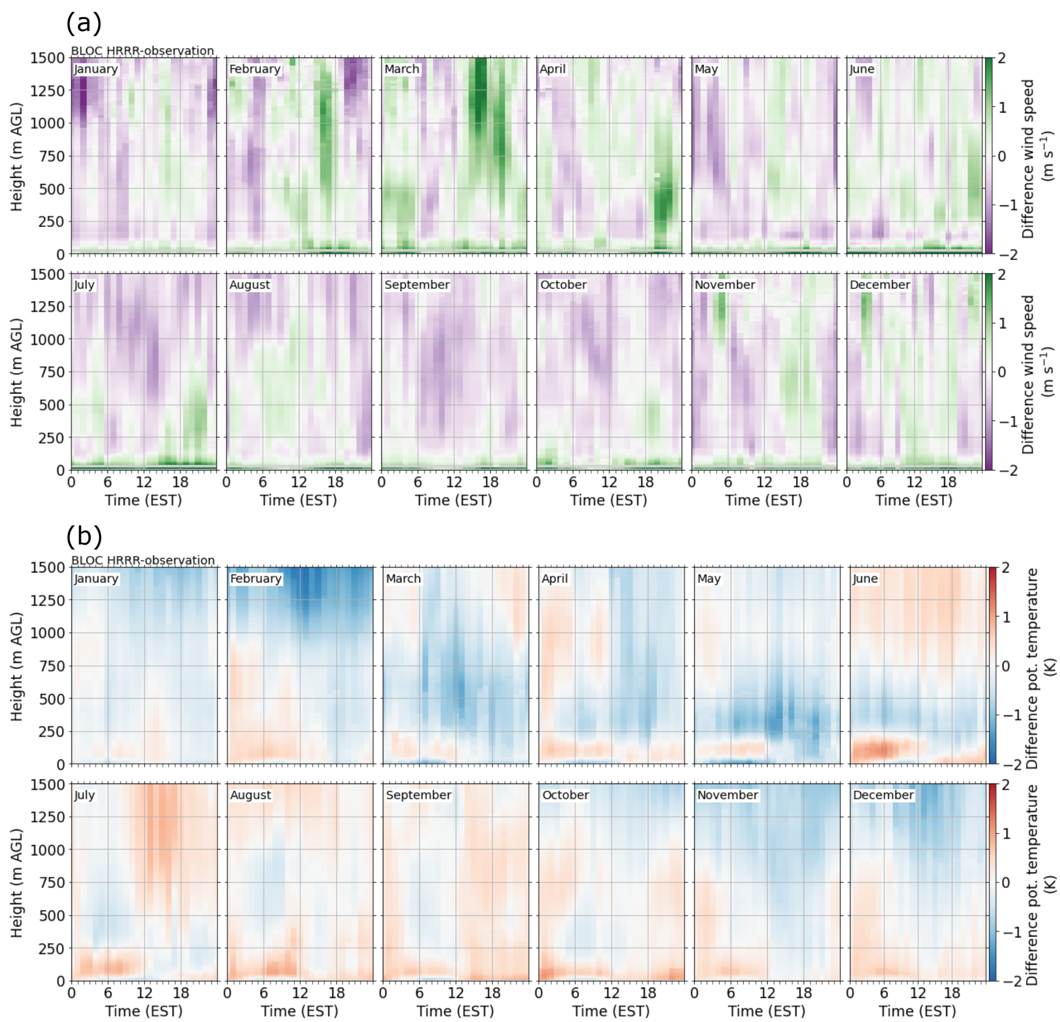

Figure S5. Monthly mean composites of HRRR model errors (model minus observation) of (a) horizontal wind speed and (b) potential temperature across the full diurnal range at BLOC. Forecast hour 12 of the HRRR model is shown. Availability had to be at least 25 % for a time/height pair to be plotted. Time is given in Eastern Standard Time (EST = UTC - 5 hours).

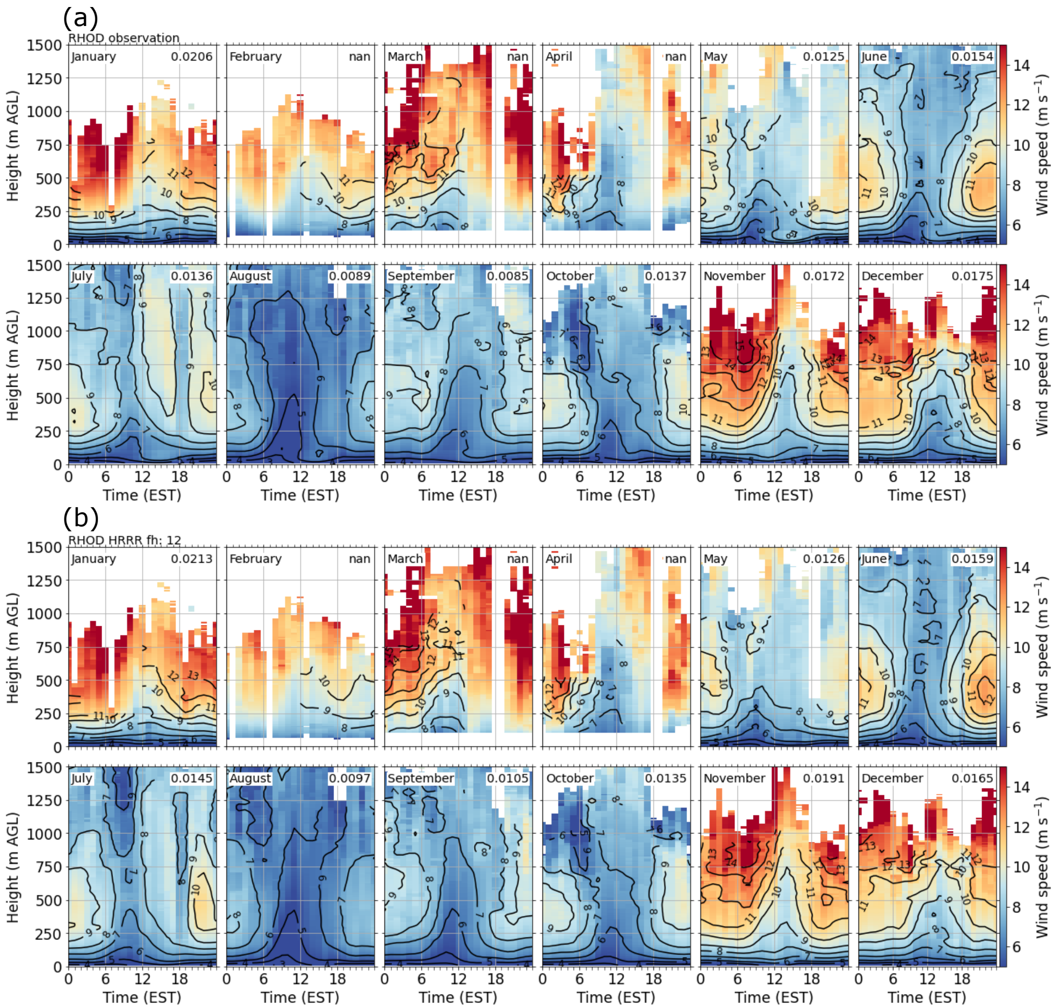

Figure S6. Monthly mean composites of (a) observed and (b) simulated horizontal wind speed (shading and contours) across the full diurnal range at RHOD. In (b), forecast hour 12 of the HRRR model is shown. Only times and heights where both model data and observations were available were used for computing the composites, and availability had to be at least 25 % for a time/height pair to be plotted. The number in the upper right corner of each subplot indicates the monthly mean shear in s^{-1} in the layer 50 to 200 m. Time is given in Eastern Standard Time (EST = UTC - 5 hours).

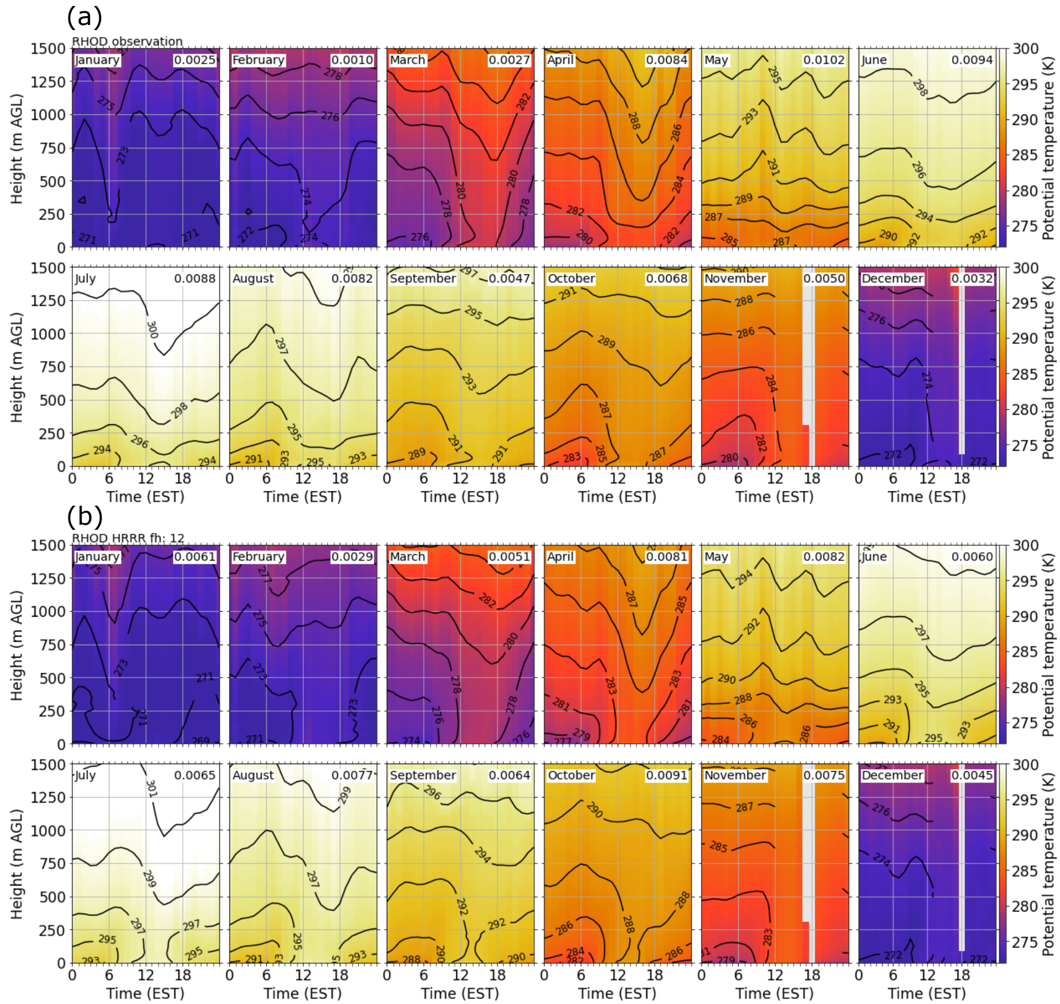

Figure S7. Monthly mean composites of (a) observed and (b) simulated potential temperature (shading and contours) across the full diurnal range at RHOD. In (b), forecast hour 12 of the HRRR model is shown. Only times and heights where both model data and observations were available were used for computing the composites, and availability had to be at least 25 % for a time/height pair to be plotted. The number in the upper right corner of each subplot indicates the monthly mean static stability in K m^{-1} in the layer 50 m to 200 m. Time is given in Eastern Standard Time (EST = UTC - 5 hours).

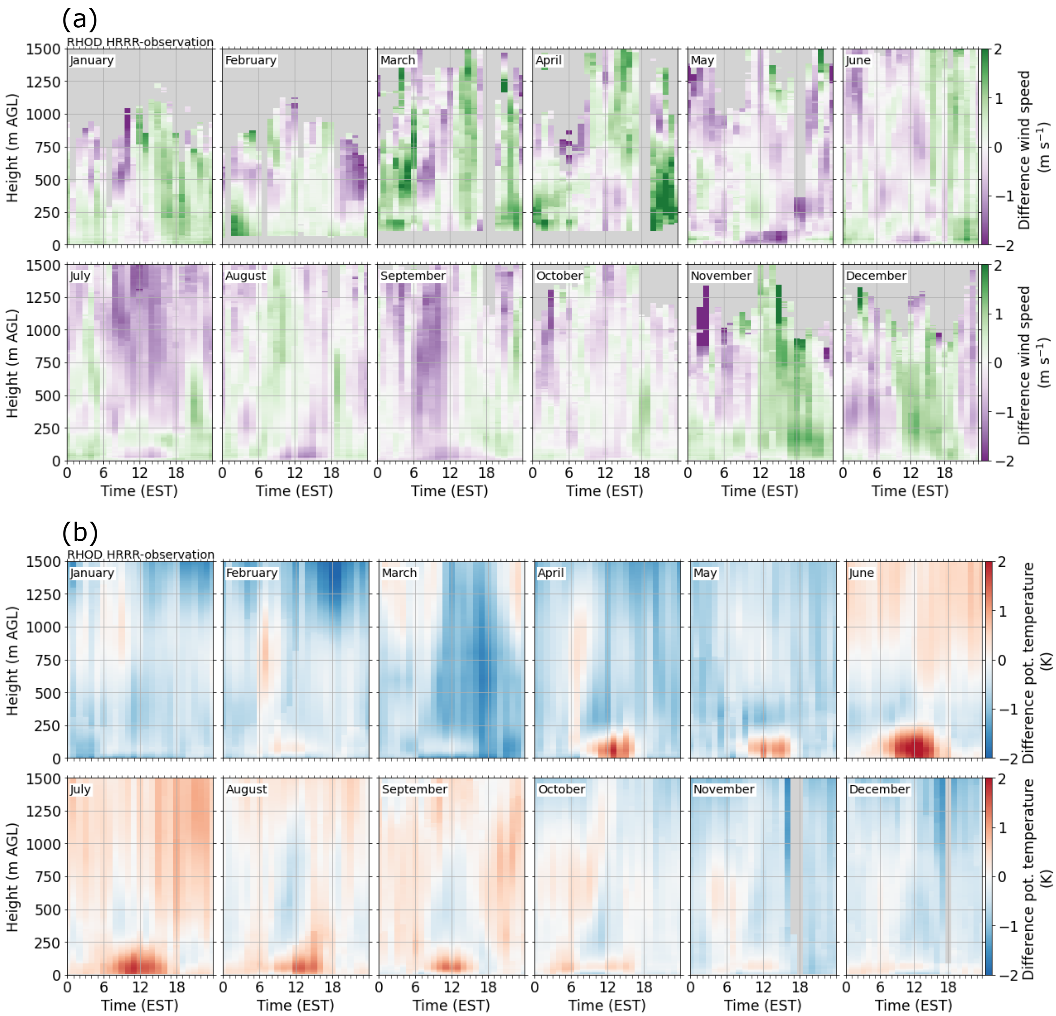

Figure S8. Monthly mean composites of HRRR model errors (model minus observation) of (a) horizontal wind speed and (b) potential temperature across the full diurnal range at RHOD. Forecast hour 12 of the HRRR model is shown. Availability had to be at least 25 % for a time/height pair to be plotted. Time is given in Eastern Standard Time (EST = UTC - 5 hours).

S5 Low-level wind speed and temperature errors in dependence of wind direction

The relationship between HRRR model errors in wind speed shear and static stability and wind direction on the y-axis is computed for BLOC (Fig. S9) and RHOD (Fig. S10).

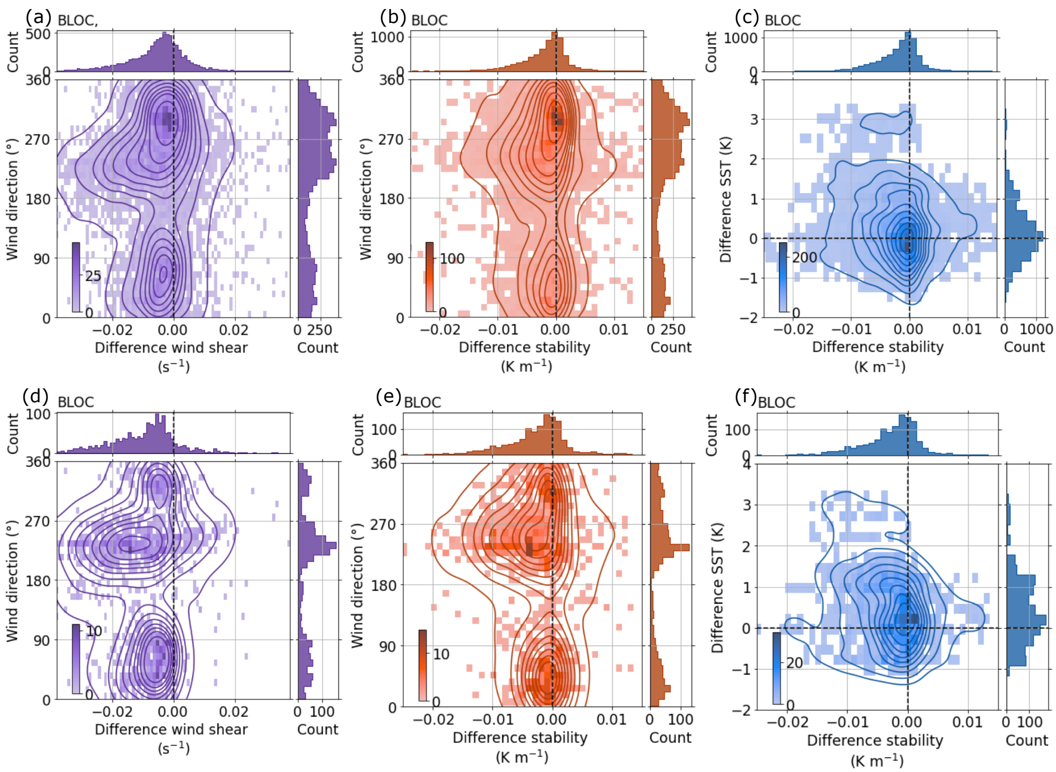

Figure S9. Relationship between the error (HRRR model minus observation) in (a,d) horizontal wind speed shear between the 50 m to 200 m layer and in (b,e) static stability computed as the virtual potential temperature gradient between 50 m and 200 m layer and observed layer-averaged wind direction at BLOC. (c,f) Relationship between the error in stability in the 50 m to 200 m layer and the error in sea surface temperature (SST) (HRRR model minus OSTIA). The top row is for all available times, and the bottom row is when an LLJ is observed. Data at forecast hour 12 are shown for the HRRR model. Marginal axes show histograms.

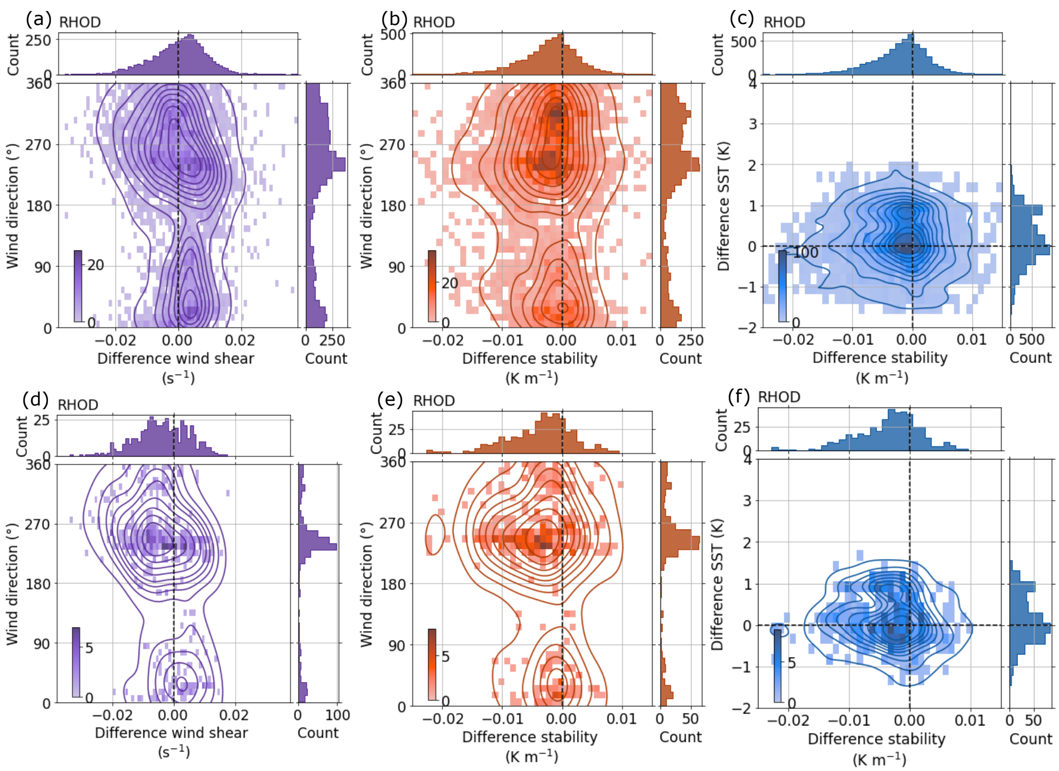

Figure S10. Relationship between the error (HRRR model minus observation) in (a,d) horizontal wind speed shear between the 50 m to 200 m layer and in (b,e) static stability computed as the virtual potential temperature gradient between 50 m and 200 m layer and observed layer-averaged wind direction at RHOD. (c,f) Relationship between the error in stability in the 50 m to 200 m layer and the error in sea surface temperature (SST) (HRRR model minus OSTIA). The top row is for all available times, and the bottom row is when an LLJ is observed. Data at forecast hour 12 are shown for the HRRR model. Marginal axes show histograms.